PERGAMON

International Journal of Solids and Structures 40 (2003) 6473–6496

INTERNATIONAL JOURNAL OF SOLIDS and STRUCTURES

www.elsevier.com/locate/ijsolstr

Adaptive multiscale wavelet-Galerkin analysis for plane elasticity problems and its applications to multiscale topology design optimization

Jae Eun Kim, Gang-Won Jang, Yoon Young Kim *

School of Mechanical and Aerospace Engineering and National Creative Research Center for Multiscale Design, Seoul National University, San 56-1, Shillim-dong, Kwanak-gu, Seoul 151-742, South Korea

Received 30 October 2002; received in revised form 4 June 2003

Abstract

The multiscale Galerkin formulation of two-dimensional elasticity problems is presented. For easy interpolation and boundary handlings as well as efficient adaptive analysis, two-dimensional interpolation wavelets are used as the multiscale trial functions in the Galerkin formulation. After the validity of the present multiscale adaptive method is verified with some benchmark problems, the present wavelet-based method is applied to the multiscale topology optimization that progresses design resolution levels dyadically from low to high levels. By this application, we show the potential of the multiscale method and the possibility of developing a fully integrated analysis and topology design optimization in the multiscale multiresolution setting.

Keywords: Multiscales; Wavelet-Galerkin analysis; Topology optimization; Multiresolution

1. Introduction

There has been an increasing interest in the wavelet-based approach in recent years due to the successes of the wavelet-based methods in several applications. Some, not all, of recent investigations on the wavelet method include papers by Amaratunga and Williams (1997), Bertoluzza and Naldi (1996), Bertoluzza (1997), Christon and Roach (2000), Cohen et al. (1998), Cohen and Masson (1999), Dahmen (2001), Glowinski et al. (1993, 1994), Kim and Jang (2002), Monasse and Perrier (1998), Wells and Zhou (1993). (See Dahmen (2001) for a recent complete list of references on this subject.) The main advantage of the wavelet-based methods is that they allow efficient adaptive analysis when analysis is carried out in multiresolution.

Though various wavelets are used as the multiscale trial basis in the Galerkin formulation, the hat interpolation wavelets are employed in this work as they have simple forms, and do not pose much

* Corresponding author. Tel.: +82-2-880-7154; fax: +82-2-883-1513.
E-mail address: yykim@snu.ac.kr (Y.Y. Kim).

0020-7683/$ - see front matter © 2003 Elsevier Ltd. All rights reserved.
doi:10.1016/S0020-7683(03)00417-7

difficulty in handling general boundary conditions especially when the wavelet-Galerkin method is formulated in a fictitious domain. Some successful applications of the interpolation wavelet-based Galerkin method are reported by Christon and Roach (2000) and Kim and Jang (2002). Christon and Roach (2000) have shown that the hat interpolation wavelets are stable in $\boldsymbol{H}^1$ and quite effective for problems with dominant elliptic characteristics. Jang et al. (2003) has recently proposed a multiscale adaptive method that can handle general boundary conditions along curved boundaries for Poisson's problems.

The first objective of the present investigation is to develop the multiscale adaptive wavelet-Galerkin method for two-dimensional plane elasticity problems by extending the approach developed by Jang et al. (2003) for Poisson's problems. The present wavelet formulation for elasticity problems will be followed by the numerical study of the typical benchmark problems. With this study, we will illustrate how efficiently two-dimensional elasticity problems are solved even with considerably small numbers of interpolation wavelet functions.

The second objective of this investigation is to apply the multiscale wavelet-Galerkin method to the multiscale topology optimization. Some advantages and effectiveness of the multiscale design optimization can be found in Kim and Yoon (2000, 2001), Earmme (2001), Poulsen (2002), and Yoon et al. (2003). Unlike the standard single-scale topology optimization, design optimization is carried out progressively from low to high resolution in the multiscale multiresolution. Since the design resolution varies, there is no need to use the same, pre-fixed analysis resolution level throughout all design resolution levels. By applying the present wavelet-Galerkin method in the adaptive multiresolution setting at every design resolution level of the multiscale design optimization, the numerical efficiency can be gained and remeshing can be avoided.

Though there still remain a few problems to overcome, the present application to the multiscale topology optimization would pave the way to the fully integrated multiscale multiresolution analysis and design optimization in the future. In standard single-scale methods, design optimization usually starts with initial fixed finite element meshes. If the analysis and design optimization are fully integrated in multiresolution, however, there will be no need to pre-select a design and/or analysis resolution level at the very beginning stage of the design optimization; the design resolution level will increase adaptively from a low to a high level sufficient enough to satisfy all the design requirements while analysis at each design iteration is carried out adaptively in multiresolution without remeshing.

In design application examples, we consider well-known compliance minimization problems. In these examples, the topology optimization is carried out in the multiscale multiresolution setting for which the present wavelet-Galerkin method will be used as an adaptive solver to avoid cumbersome remeshing. Since the history on the development of topology optimization (Bendsøe and Kikuchi, 1988) is well reviewed by Eshenauer and Olhoff (2001), the general discussion or the literature review on topology optimization will not be given here.

2. Adaptive wavelet-Galerkin analysis of two-dimensional elasticity problems

2.1. Multiscale wavelet-Galerkin formulation

We begin with the weak formulation for two-dimensional elasticity problems, which can be stated as

$$\begin{aligned} &\text{Find } \mathbf{u} \in S_\omega \quad \text{for all } \mathbf{v} \in V_\omega \\ &\int_\omega \boldsymbol{\varepsilon}(\mathbf{v}) : \mathbf{C} : \boldsymbol{\varepsilon}(\mathbf{u})\, \mathrm{d}\omega = \int_\omega \mathbf{f} \cdot \mathbf{v}\, \mathrm{d}\omega + \int_{\Gamma_\omega^h} \bar{\mathbf{t}} \cdot \mathbf{v}\, \mathrm{d}\Gamma_\omega \end{aligned} \tag{1}$$

with

$$S_\omega = \{u_i \in H^1(\omega) \,|\, u_i = g_i \text{ on } \Gamma^g_\omega\} \quad (i = 1, 2)$$
$$V_\omega = \{v_i \in H^1(\omega) \,|\, v_i = 0 \text{ on } \Gamma^g_\omega\}$$

where $\mathbf{C}$ denotes the elasticity tensor, $\boldsymbol{\varepsilon}$ the strain tensor and H^1 the Sobolev space of degree 1. The two-dimensional domain that an elastic body occupies is denoted by ω, which will be referred to as a package domain (see Fig. 1). The boundary Γ_ω of ω consists of Γ^h_ω where a surface traction $\bar{\mathbf{t}}$ is given and Γ^g_ω where displacements are prescribed.

To facilitate the adaptive multiscale analysis without remeshing, we use a rectangular fictitious domain Ω encompassing the package domain ω. The fictitious domain method has been used successfully in various problems as done by Cohen and Masson (1999), DeRose (1998), Diaz (1999), Glowinski et al. (1993, 1994), Jang et al. (2003), Wells and Zhou (1993). The boundary $\partial\Omega$ of Ω consists of three parts Γ^g_Ω, $\Gamma^{h_1}_\Omega$ and $\Gamma^{h_2}_\Omega$ such that

$$\Gamma^g_\Omega = \Omega \cap \Gamma^g_\omega, \quad \Gamma^{h_1}_\Omega = \Omega \cap \Gamma^h_\omega, \quad \Gamma^{h_2}_\Omega = \Omega \setminus (\Gamma^g_\omega \cup \Gamma^{h_1}_\omega)$$

where $\Gamma^{h_2}_\Omega$ is the traction-free boundary that does not intersect with either Γ^g_ω or $\Gamma^{h_1}_\omega$.

To formulate the multiscale method in the fictitious domain Ω, the elasticity tensor $\mathbf{C}$ and the body force $\mathbf{f}$ must be redefined as

$$\mathbf{C}_\Omega(x, y) = \begin{cases} \mathbf{C} & \text{if } (x, y) \in \omega \\ \chi\mathbf{C} & \text{else } (x, y) \in \Omega \setminus \omega \end{cases} \tag{2}$$

$$\mathbf{f}_\Omega(x, y) = \begin{cases} \mathbf{f}(x, y) & \text{if } (x, y) \in \omega \\ 0 & \text{else } (x, y) \in \Omega \setminus \omega \end{cases} \tag{3}$$

where χ is a small parameter ($\chi = 1.0 \times 10^{-3}$ is used in the present work). The effect of this parameter on the solution accuracy may be found in Cohen and Masson (1999) and Jang et al. (2003).

When the fictitious domain is introduced, the original Galerkin formulation in Eq. (1) can be approximated as

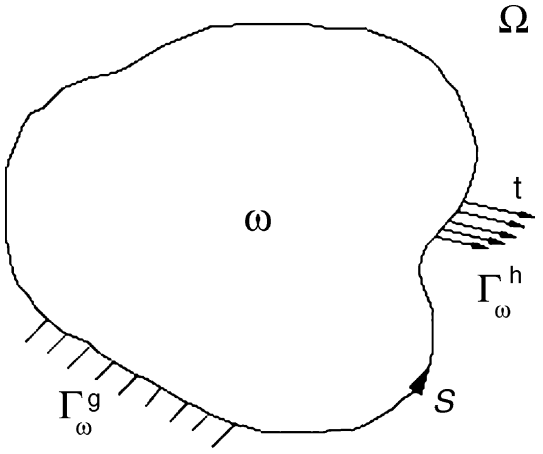

Fig. 1. The typical elasticity problem with a package domain ω embedded into a fictitious domain Ω.

$$\text{Find } \mathbf{u}_\Omega \in S_\Omega \quad \text{for all } \mathbf{v}_\Omega \in V_\Omega$$
$$\int_\Omega \boldsymbol{\varepsilon}(\mathbf{v}_\Omega) : \mathbf{C}_\Omega : \boldsymbol{\varepsilon}(\mathbf{u}_\Omega)\,\mathrm{d}\omega = \int_\Omega \mathbf{f}_\Omega \cdot \mathbf{v}_\Omega\,\mathrm{d}\Omega + \int_{\Gamma_\omega^h} \bar{\mathbf{t}} \cdot \mathbf{v}_\Omega\,\mathrm{d}\Gamma_\omega \tag{4}$$

with

$$S_\Omega = \{u_{i\Omega} \in H^1(\omega)\,|\,u_{i\Omega} = g_i \text{ on } \Gamma_\Omega^g\}$$
$$V_\Omega = \{v_{i\Omega} \in H^1(\omega)\,|\,v_{i\Omega} = 0 \text{ on } \Gamma_\Omega^g\} \quad (i = 1,2)$$

For the multiscale analysis, the displacement field $\mathbf{u}$ must be expressed in multiscales. Before presenting the full multiscale analysis, we consider the following two-scale representations of $\mathbf{u}(x,y)$ at resolution j:

$$\mathbf{u}(x,y) \simeq \mathbf{u}_j(x,y) = \begin{Bmatrix} u_j(x,y) \\ v_j(x,y) \end{Bmatrix} = \sum_{k,l} \mathbf{s}_{j,k,l}\phi_{j,k,l}(x,y) \tag{5}$$

or

$$\mathbf{u}_j(x,y) = \sum_{k,l} \mathbf{s}_{j-1,k,l}\phi_{j-1,k,l}(x,y) + \sum_{m=1}^{3}\sum_{k,l} \mathbf{d}^m_{j-1,k,l}\psi^m_{j-1,k,l}(x,y) \tag{6}$$

with

$$\mathbf{s}_{j-1,k,l} = \begin{Bmatrix} \mathbf{s}^u_{j-1,k,l} \\ \mathbf{s}^v_{j-1,k,l} \end{Bmatrix} \quad \text{and} \quad \mathbf{d}^m_{j-1,k,l} = \begin{Bmatrix} \mathbf{d}^{u,m}_{j-1,k,l} \\ \mathbf{d}^{v,m}_{j-1,k,l} \end{Bmatrix}$$

If the analysis resolution level is j for a domain $\Omega = [0,1] \times [0,1]$, for instance, the interpolating grid points will be located at $(2^{-j}k, 2^{-j}l)$ $(k,l \in \{0,1,2,\ldots,2^j\})$. The representation is the same as that used in the finite element discretization with equal-sized bilinear elements. However, the representation in Eq. (6) is given by two sets of functions $\phi_{j,k,l}$ and $\psi^m_{j,k,l}$ which are defined as

$$\phi_{j,k,l}(x,y) = 2^j\phi(2^jx - k, 2^jy - l) \tag{7}$$

$$\psi^m_{j,k,l}(x,y) = 2^j\psi^m(2^jx - k, 2^jy - l) \quad (m = 1,2,3) \tag{8}$$

The two-dimensional scaling function $\phi(x,y)$ and wavelet $\psi(x,y)$ are constructed by the tensor products of the one-dimensional hat interpolation scaling function $\phi_{1D}(x)$ and $\psi_{1D}(x)$:

$$\phi(x,y) = \phi_{1D}(x)\phi_{1D}(y)$$

$$\psi^1(x,y) = \psi_{1D}(x)\phi_{1D}(y) \quad \text{(horizontal wavelet)}$$

$$\psi^2(x,y) = \phi_{1D}(x)\psi_{1D}(y) \quad \text{(vertical wavelet)}$$

$$\psi^3(x,y) = \psi_{1D}(x)\psi_{1D}(y) \quad \text{(diagonal wavelet)}$$

The functions $\phi_{1D}(x)$ and $\psi_{1D}(x)$ are given by the autocorrelation of the Daubechies scaling function (see Beylkin and Saito, 1993) as

$$\phi_{1D}(x) = \begin{cases} x+1 & \text{for } -1 \leqslant x \leqslant 0 \\ 1-x & \text{for } 0 \leqslant x \leqslant 1 \\ 0 & \text{else} \end{cases} \tag{9}$$

$$\psi_{1D}(x) = \phi_{1D}(2x-1) = \begin{cases} 2x & \text{for } 0 \leqslant x \leqslant 1/2 \\ 2-2x & \text{for } 1/2 \leqslant x \leqslant 1 \\ 0 & \text{else} \end{cases} \tag{10}$$

If the function space generated by $\{\phi_{j,k,l}\}$ $(k,l = \text{integers})$ is denoted V_j, the use of Eq. (6) is equivalent to the decomposition of V_j into $V_{j-1} \oplus W_{j-1}$ where W_{j-1} is the space generated by $\{\psi^m_{j-1,k,l}\}$ $(k,l = \text{integers})$ that denotes the difference between V_j and V_{j-1}. Therefore, $\sum_{m=1}^{3}\sum_{k,l}\mathbf{d}^m_{j-1,k,l}\psi^m_{j-1,k,l}(x,y)$ represents the difference between $\mathbf{u}(x,y)$ in V_j and $\sum_{k,l}\mathbf{s}_{j-1,k,l}\phi_{j-1,k,l}(x,y)$ at the resolution level $j-1$.

Repeating the decomposition of V_j into V_{j-1} and W_{j-1} for $j = j_0+1,\ldots,J$ yields the following multiscale representation of $\mathbf{u}(x,y)$:

$$\mathbf{u}_j(x,y) = \sum_{k,l}\mathbf{s}_{j_0,k,l}\phi_{j_0,k,l}(x,y) + \sum_{j=j_0}^{j-1}\sum_{m=1}^{3}\sum_{k,l}\mathbf{d}^m_{j,k,l}\psi^m_{j,k,l}(x,y) \tag{11}$$

where the lowest resolution level j_0 is usually set as $j_0 = 1$. Since the scale information that each $\psi_{j,k,l}$ $(j = j_0,\ldots,J-1)$ represents is different, the representation in Eq. (11) is multiscaled. The transformation between $\{\mathbf{s}_{j,k,l}\}$ $(k,l = \text{integers})$ and $\{\mathbf{s}_{j-1,k,l}, \{\mathbf{d}^m_{j-1,k,l}\}_{m=1,2,3}\}$ $(k,l = \text{integers})$ may be represented by a transformation matrix $\boldsymbol{T}_j$, which may be found in Jang et al. (2003):

$$\{\mathbf{s}_{j,k,l}\} = \boldsymbol{T}_j \cdot \{\mathbf{s}_{j-1,k,l}, \{\mathbf{d}^m_{j-1,k,l}\}_{m=1,2,3}\}$$

To present the multiscale Galerkin formulation based on Eq. (11), we consider the following representations of $\mathbf{u}$ at the resolution j in two-scale form as in Eq. (6) and then extend the result to the full multiscale representation in Eq. (11).

In matrix form, Eq. (6) is rewritten as

$$\mathbf{u}_j(x,y) = \mathbf{N}_j(x,y)\cdot\mathbf{U}_j \tag{12}$$

where the matrix $\mathbf{N}_j$ and the coefficient vector $\mathbf{U}_j$ are defined as

$$\mathbf{N}_j(x,y) = \left[\begin{array}{cc|cc|cc|cc} \boldsymbol{\Phi}_{j-1} & 0 & \boldsymbol{\Psi}^1_{j-1} & 0 & \boldsymbol{\Psi}^2_{j-1} & 0 & \boldsymbol{\Psi}^3_{j-1} & 0 \\ 0 & \boldsymbol{\Phi}_{j-1} & 0 & \boldsymbol{\Psi}^1_{j-1} & 0 & \boldsymbol{\Psi}^2_{j-1} & 0 & \boldsymbol{\Psi}^3_{j-1} \end{array}\right] = [\,\mathbf{N}^s_j \quad \mathbf{N}^{d_1}_j \quad \mathbf{N}^{d_2}_j \quad \mathbf{N}^{d_3}_j\,] \tag{13}$$

$$\mathbf{U}_j(x,y) = \{\,\mathbf{s}^u_{j-1} \quad \mathbf{s}^v_{j-1} \quad (\mathbf{d}^{u,1}_{j-1} \quad \mathbf{d}^{v,1}_{j-1} \quad \mathbf{d}^{u,2}_{j-1} \quad \mathbf{d}^{v,2}_{j-1} \quad \mathbf{d}^{u,3}_{j-1} \quad \mathbf{d}^{v,3}_{j-1})\,\}^{\mathrm{T}} = \{\,\mathbf{s}_{j-1} \quad \mathbf{d}_{j-1}\,\}^{\mathrm{T}} \tag{14}$$

where $\mathbf{s}^\alpha_{j-1}$ and $\mathbf{d}^{\alpha,m}_{j-1}$ are defined as $\mathbf{s}^\alpha_{j-1} = \{\mathbf{s}^\alpha_{j-1,k,l}\}$, $\mathbf{d}^{\alpha,m}_{j-1} = \{\mathbf{d}^{\alpha,m}_{j-1,k,l}\}$ $(\alpha = u \text{ or } v,\ m = 1,2,3)$. The vectors $\boldsymbol{\Phi}_{j-1}, \boldsymbol{\Psi}^m_{j-1}$ in Eq. (13) may be identified by equating Eqs. (6) and (12).

Using the standard procedure employed to derive a matrix form from Eq. (1), we can derive the following matrix equation using the multiscale representation of the test and trial functions of the form in Eq. (6):

$$\mathbf{K}_j \cdot \mathbf{U}_j = \mathbf{F}_j \tag{15}$$

with

$$\mathbf{K}_j = \begin{bmatrix} \mathbf{k}^{s,s}_{j,j} & \mathbf{k}^{s,d_1}_{j,j} & \mathbf{k}^{s,d_2}_{j,j} & \mathbf{k}^{s,d_3}_{j,j} \\ & \mathbf{k}^{d_1,d_3}_{j,j} & \mathbf{k}^{d_1,d_3}_{j,j} & \mathbf{k}^{d_1,d_3}_{j,j} \\ & \text{sym} & \mathbf{k}^{d_2,d_2}_{j,j} & \mathbf{k}^{d_2,d_3}_{j,j} \\ & & & \mathbf{k}^{d_3,d_3}_{j,j} \end{bmatrix} \tag{16}$$

The submatrices $\mathbf{k}^{\beta,\gamma}_{p,q}$ in Eq. (16) are defined as

$$\mathbf{k}^{\beta,\gamma}_{p,q} = \int_\Omega (\mathbf{N}^\beta_p)^{\mathrm{T}}\mathbf{L}^{\mathrm{T}}\mathbf{D}_\Omega\mathbf{L}\mathbf{N}^\gamma_q\,\mathrm{d}\Omega \tag{17}$$

where $\mathbf{D}_\Omega$ denotes the matrix representation of the elasticity tensor $\mathbf{C}_\Omega$ and the matrix $\mathbf{N}_p^\beta$ is defined as

$$\mathbf{N}_p^\beta = \begin{cases} \mathbf{N}_p^s & \text{if } \beta = s \\ \mathbf{N}_p^{d^m} & \text{if } \beta = d^m \end{cases} \tag{18}$$

In Eq. (17), the matrix $\mathbf{L}$ denotes the usual differentiation operation:

$$\mathbf{L} = \begin{bmatrix} \dfrac{\partial}{\partial x} & \\ & \dfrac{\partial}{\partial y} \\ \dfrac{\partial}{\partial y} & \dfrac{\partial}{\partial x} \end{bmatrix}$$

We remark here that the numerical integration in Eq. (17) can be easily performed by a typical quadrature rule such as the Gauss quadrature.

The load vector $\mathbf{F}_j$ in Eq. (15) can be constructed by two parts, $\mathbf{F}_j^f$ and $\mathbf{F}_j^t$ such that

$$\mathbf{F}_j = \mathbf{F}_j^f + \mathbf{F}_j^t \tag{19}$$

where

$$\mathbf{F}_j^f = \int_\Omega \mathbf{N}_j^{\mathrm{T}} \mathbf{f}_\Omega \, \mathrm{d}\Omega \tag{20}$$

$$\mathbf{F}_j^t = \int_{\Gamma_\omega^h} \mathbf{N}_j^{\mathrm{T}} \bar{\mathbf{t}} \, \mathrm{d}\Gamma_\omega \tag{21}$$

If the usual single-scale representation of $\mathbf{u}$ at the resolution j is known

$$\mathbf{u}_j(x,y) = \sum_{k,l} \mathbf{s}_{j,k,l} \phi_{j,k,l}(x,y) \tag{22}$$

one can easily construct the system stiffness matrix $\widehat{\mathbf{K}}_j$ and the load vector $\widehat{\mathbf{F}}_j$. From these single-scale matrices $\widehat{\mathbf{K}}_j$ and $\widehat{\mathbf{F}}_j$, the present multiscale matrices $\mathbf{K}_j$ and $\mathbf{F}_j$ in Eq. (15) can be constructed by the following transform:

$$\mathbf{K}_j = \mathbf{T}_j^{\mathrm{T}} \widehat{\mathbf{K}}_j \mathbf{T}_j, \quad \mathbf{F}_j = \mathbf{T}_j^{\mathrm{T}} \widehat{\mathbf{F}}_j \quad \text{and} \quad \mathbf{U}_j = \mathbf{T}_j \widehat{\mathbf{U}}_j \tag{23a, b}$$

where $\mathbf{T}_j$ is the transformation matrix explained earlier.

To express the displacement $\mathbf{u}$ at the next resolution level $j+1$, the following multiscale representation will be used:

$$\begin{aligned} \mathbf{u}_{j+1}(x,y) &= \sum_{k,l} \mathbf{s}_{j-1,k,l} \phi_{j-1,k,l}(x,y) + \sum_{j'=j-1}^{j} \sum_{m=1}^{3} \sum_{k,l} \mathbf{d}_{j',k,l}^m \psi_{j',k,l}^m(x,y) \\ &= \mathbf{u}_j(x,y) + \sum_{m=1}^{3} \sum_{k,l} \mathbf{d}_{j,k,l}^m \psi_{j,k,l}^m(x,y) \end{aligned} \tag{24}$$

Considering the additional contribution of $\sum_{m=1}^{3} \sum_{k,l} \mathbf{d}_{j,k,l}^m \psi_{j,k,l}^m(x,y)$ for the resolution $j+1$, one can express the stiffness matrix $\mathbf{K}_{j+1}$ in the following form:

$$\mathbf{K}_{j+1} = \begin{bmatrix} \mathbf{k}_{j+1}^{s,s} & \mathbf{k}_{j+1}^{s,d} \\ \text{sym} & \mathbf{k}_{j+1}^{d,d} \end{bmatrix}$$

Since $\mathbf{k}_{j+1}^{s,s} = \mathbf{K}_j$, only $\mathbf{k}_{j+1}^{s,d}$ and $\mathbf{k}_{j+1}^{d,d}$ need to be newly constructed. The procedure to construct $\mathbf{k}_{j+1}^{s,d}$ and $\mathbf{k}_{j+1}^{d,d}$ is similar to that used to construct $\mathbf{K}_j$.

By carrying out the process described above for from the lowest resolution $j = j_0$ to the highest resolution J, the following system equation can be finally formed:

$$\mathbf{K}_J \cdot \mathbf{U}_J = \mathbf{F}_J \tag{25}$$

where

$$\mathbf{U}_J = \{\mathbf{s}_{j_0}^u, \mathbf{d}_{j_0}^u, \mathbf{d}_{j_0+1}^u, \ldots, \mathbf{d}_{J-1}^u\}^{\mathrm{T}} \tag{26}$$

and

$$\mathbf{F}_J = \{\mathbf{s}_{j_0}^F, \mathbf{d}_{j_0}^F, \mathbf{d}_{j_0+1}^F, \ldots, \mathbf{d}_{J-1}^F\}^{\mathrm{T}} \tag{27}$$

and $\mathbf{K}_J$ can be constructed by the same procedure to form $\mathbf{K}_{j+1}$ from $\mathbf{K}_j$. More detailed procedures for Poisson's problems can be found in Christon and Roach (2000) and Jang et al. (2003).

2.2. Treatment of boundary conditions

The prescription of boundary conditions along curved boundaries has been one of the major difficulties in developing an efficient multiscale wavelet-Galerkin method for problems defined in non-rectangular domains. By extending the technique proposed for Poisson's problems, we develop a method to handle boundary conditions along general boundary curves for plane elasticity problems.

In this work, the boundary $\partial\omega$ of the package domain inside Ω is represented by zigzag lines. Fig. 2(b) illustrates the zigzag approximation of the original boundary shown in Fig. 2(a). The grid size shown in Fig. 2 governs the resolution or the precision of the approximation used. If the area fraction of a rectangular cell lying on ω is greater than that lying on $\Omega \setminus \omega$, the cell is declared to lie inside the package domain Ω. The approximated package domain and its boundary will be denoted by ω_{A} and $\partial\omega_{\mathrm{A}}$, respectively.

To prescribe the displacement or the traction boundary conditions, it is convenient to work with either $\widehat{\mathbf{U}}_j$ or $\widehat{\mathbf{F}}_j$, the single-scale representations of the displacement and load vectors. To prescribe $u_i = g_i$ $(i = 1, 2)$ along $\Gamma_{\omega_{\mathrm{A}}}^g$, the value of g_i on the point of Γ_{ω}^g closest to $\Gamma_{\omega_{\mathrm{A}}}^g$ are used and simply substituted into the

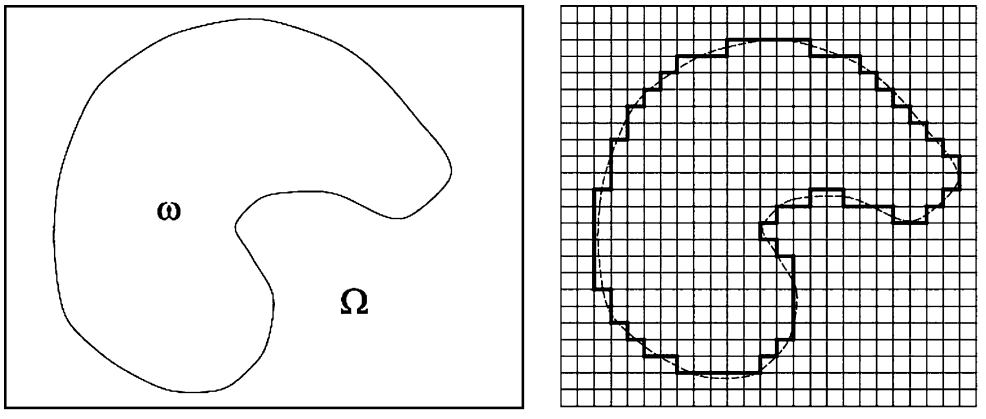

(a) (b)

Fig. 2. (a) The package domain ω with a general boundary and (b) its approximated domain ω_{A} with zigzag lines.

corresponding locations in $\widehat{\mathbf{U}}_j$. Then, its multiscale form $\mathbf{U}_j$ is obtained from $\widehat{\mathbf{U}}_j$ by the successive applications of $\boldsymbol{T}_j$.

To treat traction boundary conditions, consider a traction vector $\mathbf{t}(s)$ prescribed along Γ^h_ω in Fig. 3(a). As in displacement boundary conditions, when approximating the boundary as $\Gamma^h_{\omega_\mathrm{A}}$ that consists of zigzag lines, one can approximate the force vector $\widehat{\mathbf{F}}^t_j$ as

$$\widehat{\mathbf{F}}^t_j = \int_{\Gamma^h_\omega} \widehat{\mathbf{N}}^{\mathrm{T}}_j \mathbf{t}(s)\,\mathrm{d}s = \int_{\Gamma^h_\omega} \widehat{\mathbf{N}}^{\mathrm{T}}_j (\mathbf{t}(s)\sin\theta\,\mathrm{d}x + \mathbf{t}(s)\cos\theta\,\mathrm{d}y) \tag{28}$$

where $\widehat{\mathbf{N}}_j$ denotes the single-scale version of $\mathbf{N}_j$ in Eq. (13).

To transfer the traction boundary conditions prescribed on $\partial\omega$ into those prescribed on the approximate boundary condition $\partial\omega_\mathrm{A}$, the following approximation is considered:

$$\widehat{\mathbf{F}}^t_j \approx \int_{\Gamma^h_{\omega_\mathrm{A}}} \widehat{\mathbf{N}}^{\mathrm{T}}_j (\mathbf{t}(s)\sin\theta\,\mathrm{d}x + \mathbf{t}(s)\cos\theta\,\mathrm{d}y) = \int_{\Gamma^h_{\omega_\mathrm{A}}} \widehat{\mathbf{N}}^{\mathrm{T}}_j (\mathbf{t}^V_\mathrm{A}(x)\,\mathrm{d}x + \mathbf{t}^H_\mathrm{A}(y)\,\mathrm{d}y) \tag{29}$$

with

$$\mathbf{t}^V_\mathrm{A}(x) = \mathbf{t}(s)\sin\theta, \quad \mathbf{t}^H_\mathrm{A}(y) = \mathbf{t}(s)\cos\theta \tag{30}$$

where the arc coordinate s, the angle θ and the unit normal vector $\mathbf{n}$ are depicted in Fig. 3(a) and (b). The approximation in Eq. (20) is to replace $\mathbf{t}(s)$ by a statically equivalent system consisting of $\mathbf{t}^V_\mathrm{A}$ and $\mathbf{t}^H_\mathrm{A}$ as

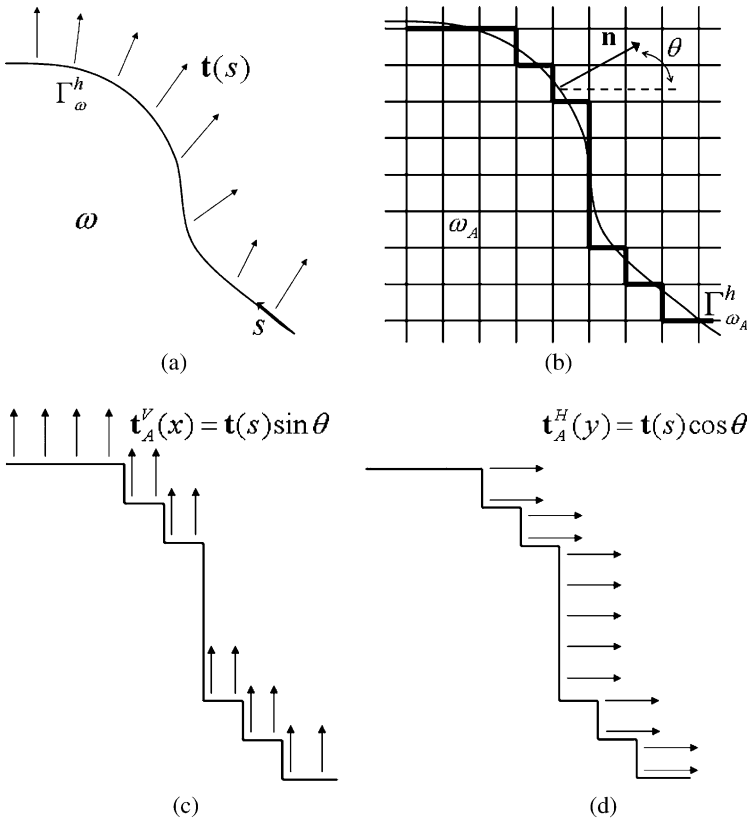

Fig. 3. (a) A general boundary Γ^h_ω under a surface reaction (b) its approximated boundary $\Gamma^h_{\omega_\mathrm{A}}$ with zigzag lines and (c,d) a statically equivalent system.

illustrated in Fig. 3(c) and (d). Other approximations are possible, but the present approximation is not only simple but also effective as shall be seen later with numerical examples. Once $\widehat{\mathbf{F}}_j^t$ is determined by Eq. (29), its multiscale version $\mathbf{F}_j^t$ is obtained through the transformation $\boldsymbol{T}_j$.

2.3. Adaptive strategy

In the wavelet-based analysis, the wavelet coefficients in $\mathbf{U}_j$ represent the differences between low and high resolution approximations. Consequently, this method possesses an intrinsic adaptivity. Cohen et al. (1998) and Dahmen (2001) presented efficient adaptive schemes using (bi-)orthogonal wavelets and showed that the convergence rate is asymptotically optimal. Kim and Jang (2002) and Jang et al. (2003) have recently investigated the convergence property of the adaptive hat wavelet-based Galerkin method numerically for one-dimensional box beam problems and two-dimensional Poisson problems.

In this work, we will use the adaptive scheme using two thresholding parameters ($\varepsilon^u > \varepsilon^l > 0$). Assume that the analysis at the resolution level $j+1$ (with $\{\phi_{j_0,k,l}, \{\psi^m_{j',k,l}\}_{j'=j_0,\ldots,j}\}$) is finished. Then the following procedures are used for the adaptive analysis at the next resolution level $j+2$:

(i) Exclude the wavelet $\psi^m_{j,k,l}$ from the basis set if its coefficient $|\mathbf{d}^m_{j,k,l}| < \varepsilon^l_j$ (31a)

(ii) Preserve $\psi^m_{j,k,l}$ in the basis set if $\varepsilon^l_j \leqslant |\mathbf{d}^m_{j,k,l}| \leqslant \varepsilon^u_j$ (31b)

(iii) Add child wavelets of $\psi^m_{j,k,l}$ into the basis set if $|\mathbf{d}^m_{j,k,l}| > \varepsilon^u_j$ (31c)

In (31), the child wavelets $\psi^m_{j+1,k,l}$ are the wavelets at resolution $j+2$ having the corresponding interpolation points near those of the parent wavelet $\psi^m_{j,k,l}$. The interpolation points for three types of the child wavelets are illustrated in Fig. 4. As the resolution level increases, the thresholding parameters are usually reduced as $\varepsilon^u_{j+1} = \varepsilon^u_j/2$ and $\varepsilon^l_{j+1} = \varepsilon^l_j/2$.

The flow chart of the overall sequence of the present adaptive scheme is shown in Fig. 5. In applying the adaptive scheme, two strategies illustrated in Fig. 6 can be considered. To explain these strategies, we utilize a simple one-dimensional analysis model. In Strategy A, the adaptive scheme (31) is applied to the interpolation wavelets having the finest scales at the current resolution level. On the other hand, Strategy B considers all leaf wavelets, regardless of their scales. The leaf wavelets are defined as the wavelets having no child wavelet, and indicated by the dotted line in Fig. 6(b).

Although Strategy A is simple to implement, it has some deficiency; once some wavelets are declared not to have child wavelets at a certain level, those wavelets are not allowed to have child wavelets any more. Therefore, no further refinement is permitted around the interpolation (or grid) points of these wavelets.

On the other hand, further refinement can be made at any location if the condition (31c) is satisfied since all leaf wavelets are examined in Strategy B at every resolution level. The flow chart for Strategy B is shown in Fig. 7 where parameters η and γ are small positive numbers and $j_{\max}$ is the maximum resolution level allowed. In the multiscale multiresolution method, the solution at resolution level j is used as an initial guess for the next higher resolution level.

2.4. Numerical verifications

In this section, we will consider two benchmark-type problems to show the effectiveness of the present multiscale analysis method.

Case Study 1: Short cantilever beam

As the first case, a square cantilever beam in Fig. 8 is considered. The numerical data are: p (pressure) $= 1000$, E (Young's modulus) $= 2.0\times10^8$, v (Poisson's ratio) $= 0.3$. Fig. 9 shows the error energy norms

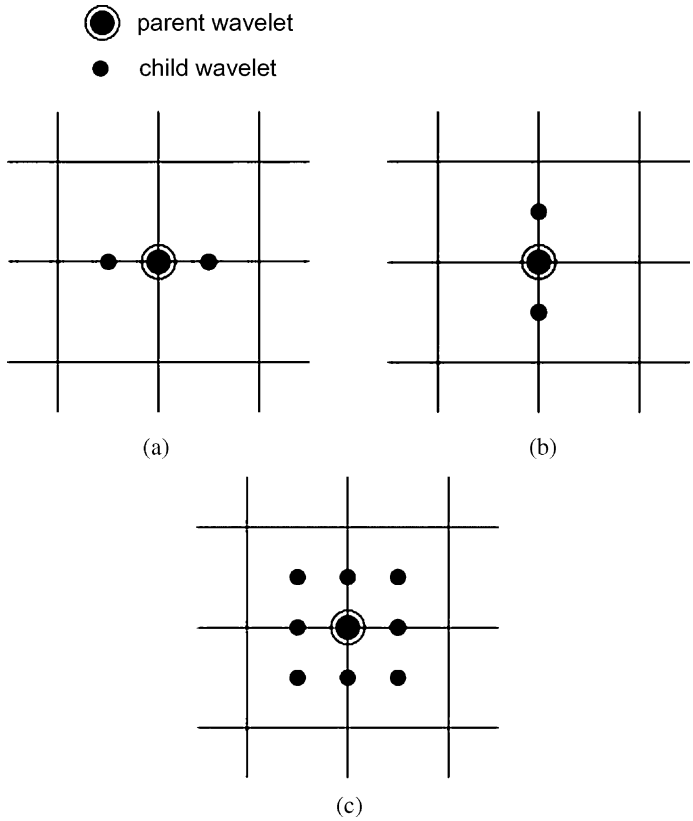

Fig. 4. The interpolation (grid) points of the child wavelets $\psi^m_{j+1,k,l}$: (a) for the horizontal wavelet ($m = 1$), (b) for the vertical wavelet ($m = 2$), and (c) for the diagonal wavelet ($m = 3$).

(e) obtained by the non-adaptive (A) and adaptive (B) schemes. The well-known stress recovery technique (Zienkiewicz and Zhu, 1992) is applied to measure the error energy norm. For the error analysis, the present multiscale result is transformed into a single scale form.

Fig. 9 shows that the results by the adaptive methods (Strategies A and B) converge faster than the result by the non-adaptive method. However, the numerical efficiency of Strategy A is very low; the magnitude of the error energy norm by Strategy A is almost the same as that by the non-adaptive method as the resolution level increases. This is because the refinement near the interpolation points of the wavelets to which no child wavelet was added at the previous resolution level is not allowed at any higher resolution level.

The locations of the interpolation points of wavelets at the final level are shown in Fig. 10(a) and (b) for Strategies A and B, respectively. Because of the deficiency of Strategy A mentioned earlier, unnecessarily many interpolation points were used for the case of Strategy A.

Case 2: Rectangular panel with a circular hole

As the next example, a stress concentration problem shown in Fig. 11 is considered. Fig. 11 depicts a quarter of a panel having a hole of radius $r = 0.1$ at its center. The uniform tension $p = 1000$ in the vertical direction is applied on the top and bottom edges of the panel. To treat the circular boundary of the hole, the fictitious domain approach is applied. Since Strategy B always works better than Strategy A, only Strategy B will be used for all the remaining numerical problems.

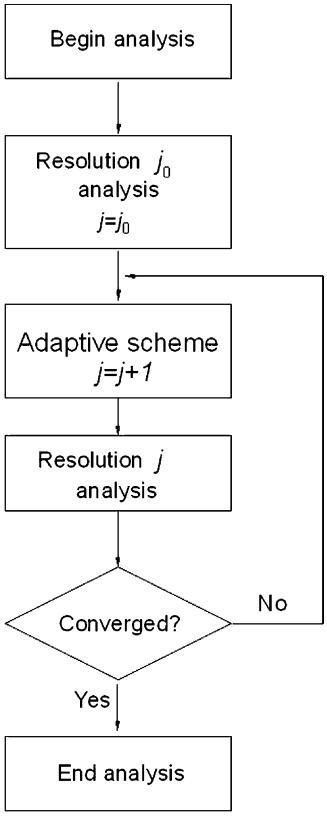

Fig. 5. The flow chart for the adaptive scheme.

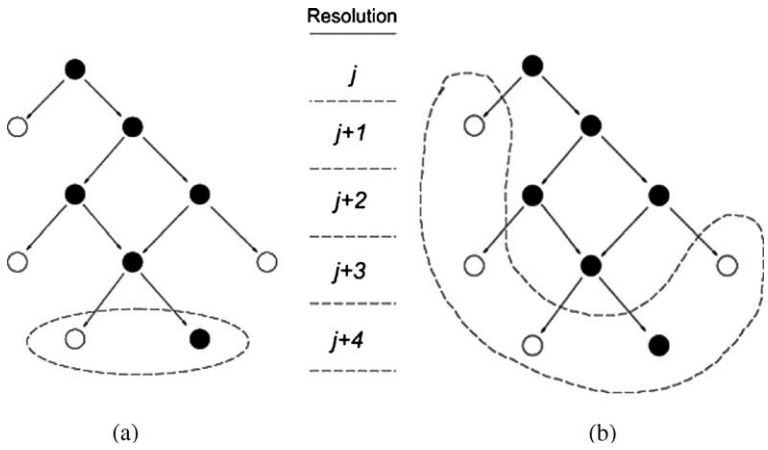

Fig. 6. Two adaptive schemes: (a) Strategy A and (b) Strategy B.

Fig. 12 shows the stress distribution along $\overline{AB}$ of the quarter panel. The solution obtained by the present adaptive wavelet-Galerkin method agrees well with the converged result by the finite element package,

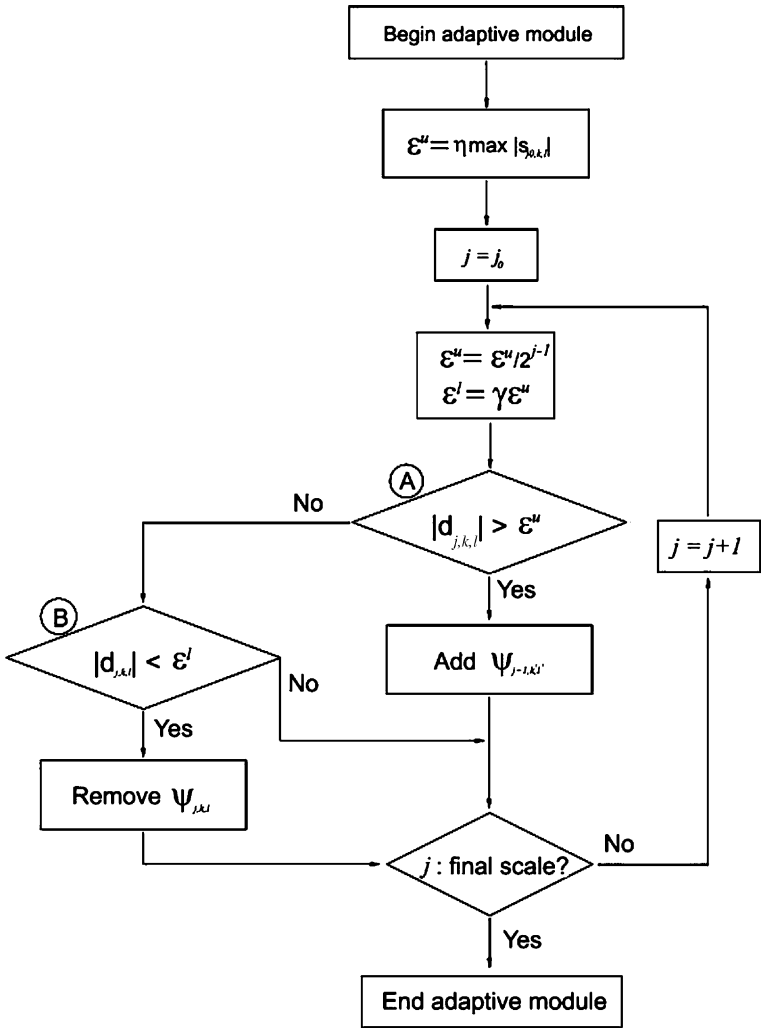

Fig. 7. The adaptive scheme for Strategy B.

ANSYS (12,053 PLANE42 elements). This solution also agrees favorably with the analytic solution for an infinite panel with a hole.

Fig. 13 shows the location of interpolation points that are adaptively added by Strategy B. Since stress is concentrated around the hole, the density of the interpolation points is high around it. It is also noted that some interpolation wavelet points lie outside the original package domain. In the fictitious domain method, we must consider all the wavelets defined on Ω affecting the solution inside the package domain ω. More specifically, wavelets whose interpolation points are on $\Omega \setminus \omega$ and lie across $\partial\omega$ must be considered in the analysis.

3. Application to the multiscale multiresolution topology optimization

In this section, the multiscale wavelet-Galerkin method will be applied to the multiscale multiresolution topology optimization. The topology optimization formulation (Bendsøe and Kikuchi, 1988) for compli-

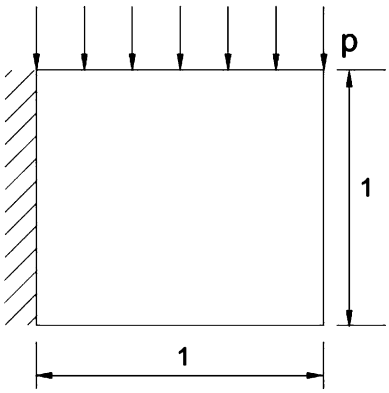

Fig. 8. The short cantilever beam under uniform pressure.

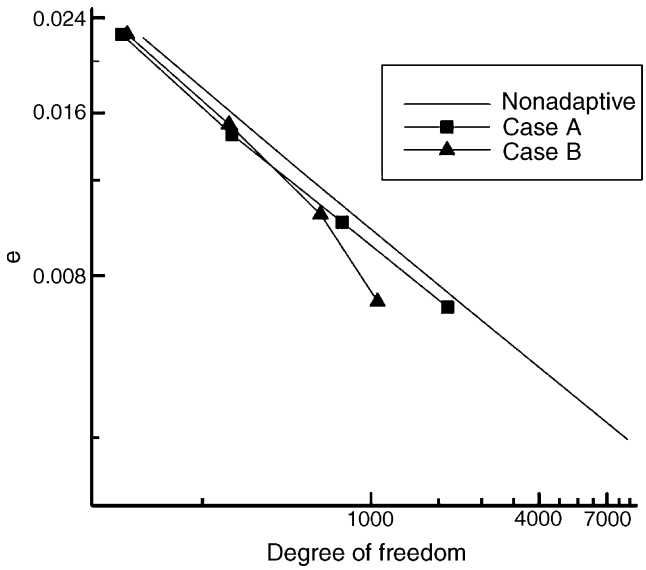

Fig. 9. The comparison of the error energy norms by the non-adaptive method and adaptive schemes, Strategy A and Strategy B.

ance minimization will be briefly stated. Then, the multiscale topology optimization using the standard single-scale finite element analysis will be given. The main development in this section is to show how the multiscale wavelet-Galerkin method can be incorporated in the multiscale optimization formulation.

3.1. Topology optimization formulation for compliance minimization

Topology optimization problems for minimizing the structural mean compliance for a prescribed amount of material can be formulated by the density function method (Bendsøe, 1995) as

$$\text{Minimize } f(\boldsymbol{\rho}) = \widehat{\mathbf{U}}_j^{\mathrm{T}}(\boldsymbol{\rho})\widehat{\mathbf{K}}_j(\boldsymbol{\rho})\widehat{\mathbf{U}}_j(\boldsymbol{\rho}) \tag{32}$$

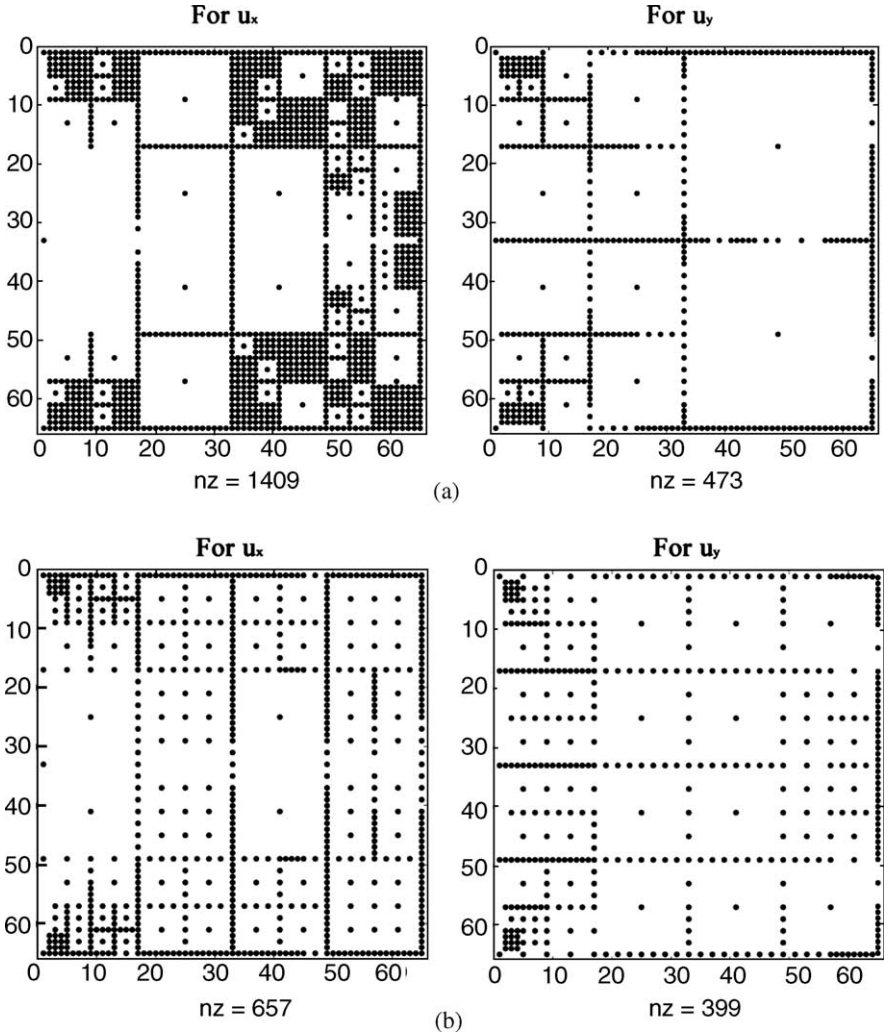

Fig. 10. Grid point locations of the interpolation wavelets by (a) Strategy A and (b) Strategy B.

$$\text{subject to a mass constraint } h(\boldsymbol{\rho}) = \sum_{e=1}^{N_e} \int_{\Omega_e} \rho_e \, \mathrm{d}\Omega - M_0 \leqslant 0 \tag{33}$$

$$\text{side constraints } \varepsilon \leqslant \rho_e \leqslant 1 \ (0 < \varepsilon \ll 1) \tag{34}$$

In Eq. (32), $\boldsymbol{\rho}$ denotes $\{\rho_1, \rho_2, \ldots, \rho_e, \ldots, \rho_{N_e}\}^{\mathrm{T}}$ and N_e is the number of finite elements in a design domain and V_e, the volume of each element.

Here, we begin with the usual single-scale representation of the topology optimization formulation. The single-scale stiffness matrix $\widehat{\mathbf{K}}_j$ is regarded as the function of the density variable $\boldsymbol{\rho}$ through the following SIMP model (see Bendsøe and Sigmund, 1999, for details on this type of modeling) in the single-scale element stiffness level:

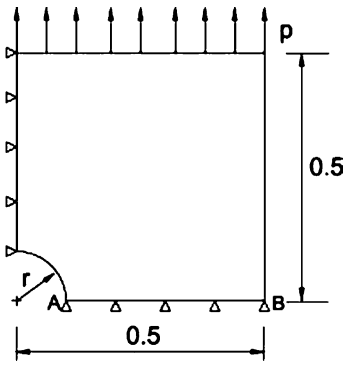

Fig. 11. Quarter model of a plate with a center hole. The plate is under uniform uniaxial tension ($r = 0.1$).

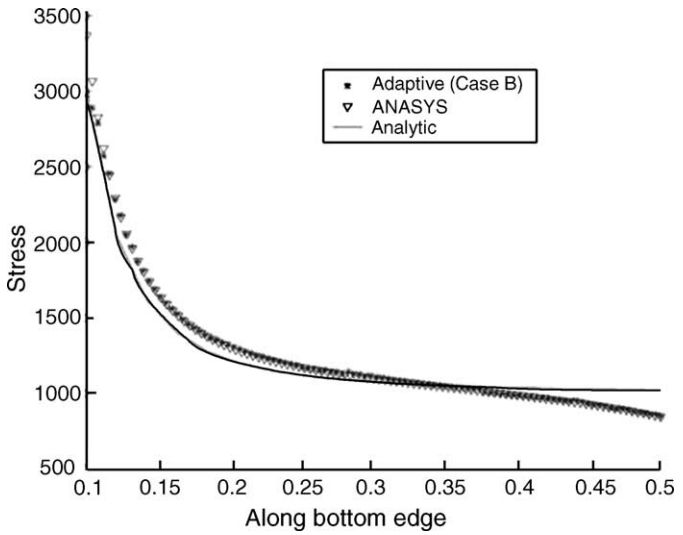

Fig. 12. Stress plot along the bottom edge $\overline{AB}$ depicted in Fig. 11.

$$\mathbf{D} = \mathbf{D}(\rho_e) = (\rho_e)^n \mathbf{D}_0 \tag{35}$$

where $\mathbf{D}_0$ is the elasticity matrix of the given isotropic material.

The sensitivity of f and h with respect to ρ_e are simply found as

$$\frac{\partial f(\boldsymbol{\rho})}{\partial \rho_e} = -\widehat{\mathbf{U}}_j^{\mathrm{T}} \frac{\partial \widehat{\mathbf{K}}_j}{\partial \rho_e} \widehat{\mathbf{U}}_j = -\hat{\mathbf{u}}_{je}^{\mathrm{T}} \frac{\partial \widehat{\mathbf{k}}_{je}}{\partial \rho_e} \hat{\mathbf{u}}_{je} = -\frac{n}{\rho_e} \hat{\mathbf{u}}_{je}^{\mathrm{T}} \widehat{\mathbf{k}}_{je} \hat{\mathbf{u}}_{je} \tag{36}$$

$$\frac{\partial h(\boldsymbol{\rho})}{\partial \rho_e} = V_e \tag{37}$$

To compute $f(\boldsymbol{\rho})$ and $\partial f(\boldsymbol{\rho})/\partial \rho_e$, the standard single-scale finite element is used.

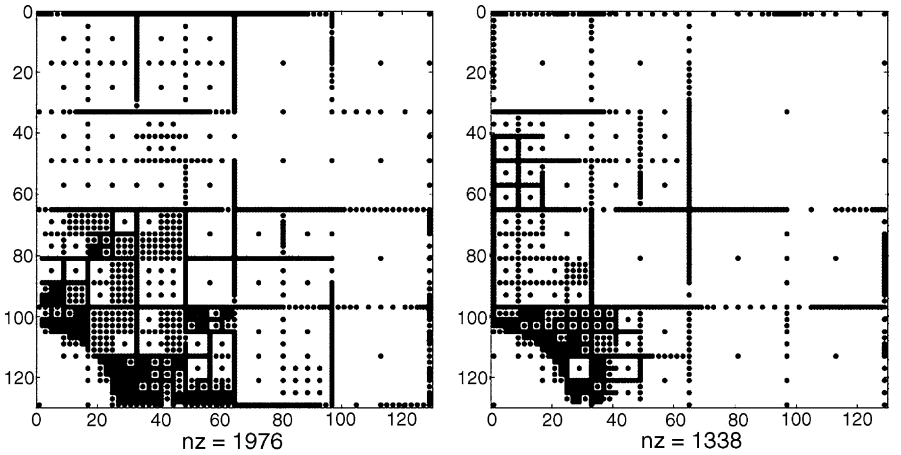

Fig. 13. The location of the grid points of wavelets for the solution in Example 2: (a) for the horizontal displacement u^x and (b) for the vertical displacement u^y.

3.2. Multi-scale topology optimization using single-scale finite element analysis

In the multiscale topology optimization, the design variables are not the single-scale density variables $\boldsymbol{\rho}$, but multiscaled variables $\mathbf{w}$. Once the design variables are expressed in multiscale, design optimization can be carried out in multiresolution.

Following Kim and Yoon (2000), the single-scale density variables $\boldsymbol{\rho}$ are first transformed to the single-scale auxiliary variables $\boldsymbol{\xi}$ as

$$\rho_e = \frac{1}{1+\exp(-S\cdot\xi_e)} \quad (-\infty < \xi_e < \infty) \tag{38}$$

The role of the nonlinear transform of Eq. (38) is to eliminate the side constraints in Eq. (34), which otherwise become complicated constraints in the multiscale design space. For the subsequent analysis, we assume that the original single-scale density variables are defined on equal-sized finite elements.

The auxiliary variables $\boldsymbol{\xi}$ are then transformed into the multiscale variables $\mathbf{w}$ by means of the two-dimensional Haar wavelet transform $\mathbf{T}^H_{j_D}$ (see e.g., Mallat, 1998):

$$\mathbf{w}_{j_D} = \mathbf{T}^H_{j_D}\cdot\boldsymbol{\xi}_{j_D} \quad (-\infty < w_i < \infty) \tag{39}$$

The subscript j_D denotes the design resolution level. For instance, if the design domain is discretized by $2^m \times 2^n$ elements, j_D is $\min(m,n)$.

The transformation from $\boldsymbol{\xi}$ to $\mathbf{w}$ is equivalent to changing the basis of the design variables. In case of a domain discretized by 2×2 finite elements ($j_D = 1$) for example, the single-scale and the multiscale bases are graphically depicted in Fig. 14. In Fig. 14, ${}^H\phi$, ${}^H\psi^i$ are the Haar scaling function and wavelets. The meaning of the right superscript i is the same as that used for the interpolation wavelet systems. In the present applications, we use the non-standard Haar wavelets (see Stollnitz et al., 1996) which have a better space localization property than the standard Haar wavelets.

The sensitivity of f with respect to the multiscale design variables $\mathbf{w}$ can be determined from the following equation:

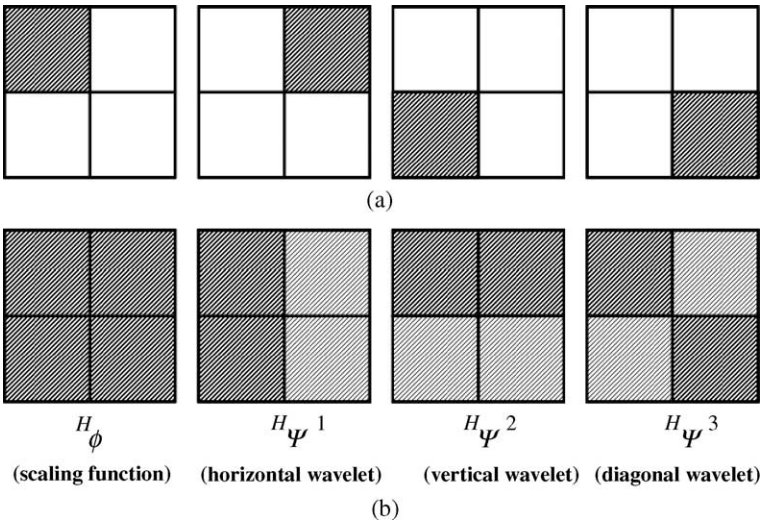

Fig. 14. Graphical illustration of the design variable basis for (a) single-scale and (b) multiscale representations (▨: +1, ▨: −1, □: 0).

$$\frac{\partial f}{\partial w_i} = \sum_{k=1}^{N_e} \frac{\partial f}{\partial \rho_k} \frac{\partial \rho_k}{\partial \xi_k} \frac{\partial \xi_k}{\partial w_i}$$

i.e.,

$$\frac{\partial f}{\partial \mathbf{w}} = \mathbf{T}^H_{J_D} \frac{\partial \boldsymbol{\rho}}{\partial \boldsymbol{\xi}} \frac{\partial f}{\partial \boldsymbol{\rho}} \tag{40a}$$

$$\left[\frac{\partial \boldsymbol{\rho}}{\partial \boldsymbol{\xi}}\right]_{ij} = \frac{S\mathrm{e}^{-S\xi_i}}{\left(1+\mathrm{e}^{-S\xi_i}\right)^2}\delta_{ij} \tag{40b}$$

The sensitivity of h with respect to $\mathbf{w}$ has the same form as Eq. (40).

Once the design variables are expressed in multiscales, the topology optimization can be carried out in multiresolution from $j_D = 1$ to $j_D = J_D$. For the case of the design optimization over two resolution levels from the lowest level $j_D = 1$ to the highest level $j_D = 2$, for instance, the design space decompositions for $j_D = 1$ and $j_D = 2$ are illustrated in Fig. 15. The coefficients ${}^H\mathbf{s}_{j_D}$ and ${}^H\mathbf{d}^i_{j_D}$ $(i = 1, 2, 3)$ are the Haar scaling and wavelet coefficients corresponding to ${}^H\phi_{j_D}$ and ${}^H\psi^i_{j_D}$ $(i = 1, 2, 3)$, respectively. In terms of ${}^H\mathbf{s}_{j_D}$ and ${}^H\mathbf{d}^i_{j_D}$, the variables $\mathbf{w}$ can be arranged as

$$\mathbf{w}_{J_D} = \left[{}^H\mathbf{s}_{j_{D0}}, ({}^H\mathbf{d}^1_{j_{D0}}, {}^H\mathbf{d}^2_{j_{D0}}, {}^H\mathbf{d}^3_{j_{D0}}), ({}^H\mathbf{d}^1_{j_{D0}+1}, {}^H\mathbf{d}^2_{j_{D0}+1}, {}^H\mathbf{d}^3_{j_{D0}+1}), \ldots, ({}^H\mathbf{d}^1_{J_D-1}, {}^H\mathbf{d}^2_{J_D-1}, {}^H\mathbf{d}^3_{J_D-1})\right]^{\mathrm{T}} \tag{41}$$

In the multiresolution design setting, the optimized design at a certain resolution, say $j_D = 1$, is used as an initial guess for the design optimization at the next resolution, say $j_D = 2$. Since the design variables are expressed in multiscales, the values of the design variables at $j_D = 1$ are directly used for the design at $j_D = 2$.

3.3. Multiscale analysis for multiscale topology optimization

In this section, we apply the adaptive multiscale wavelet-Galerkin method for numerical analysis during the multiscale topology design optimization. With this application, the design resolution increases until the

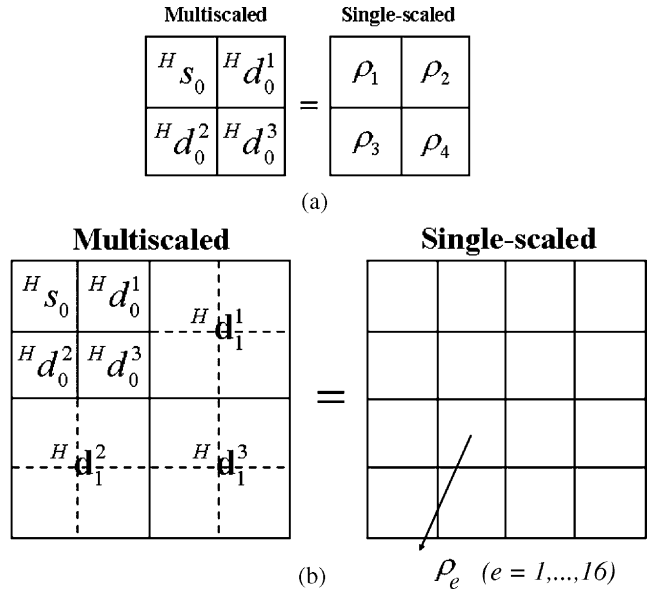

Fig. 15. The multiscale design space decompositions for (a) $j_D = 1$ and (b) $j_D = 2$.

desired design resolution level is reached while the analysis resolution for each design resolution is "adaptively" adjusted by means of the multiscale wavelet-Galerkin method.

To this end, we rewrite the objective function f in Eq. (32) in multiscale form:

$$f = \widehat{\mathbf{U}}_j^{\mathrm{T}}(\boldsymbol{\rho})\widehat{\mathbf{K}}_j(\boldsymbol{\rho})\widehat{\mathbf{U}}_j(\boldsymbol{\rho}) = \mathbf{U}_j^{\mathrm{T}}(\boldsymbol{\rho})\mathbf{K}_j(\boldsymbol{\rho})\mathbf{U}_j(\boldsymbol{\rho}) = \mathbf{U}_j^{\mathrm{T}}(\boldsymbol{\rho}(\mathbf{w}))\mathbf{K}_j(\boldsymbol{\rho}(\mathbf{w}))\mathbf{U}_j(\boldsymbol{\rho}(\mathbf{w})) \tag{42}$$

Here, the design variables are the multiscale variables $\mathbf{w}$ and the nodal displacements and the system stiffness matrix are also multiscaled by means of the two-dimensional interpolation wavelets.

To find the sensitivity of f of Eq. (42) with respect to $\mathbf{w}$, we first express $\partial f/\partial \boldsymbol{\rho}$ as

$$\frac{\partial f}{\partial \rho_e} = -\widehat{\mathbf{U}}_j^{\mathrm{T}}\frac{\partial \widehat{\mathbf{K}}_j}{\partial \rho_e}\widehat{\mathbf{U}}_j = -\mathbf{U}_j^{\mathrm{T}}\mathbf{T}_j^{\mathrm{T}}\frac{\partial \widehat{\mathbf{K}}_j}{\partial \rho_e}\mathbf{T}_j\mathbf{U}_j = -\mathbf{u}_{je}^{\mathrm{T}}\mathbf{T}_{je}^{\mathrm{T}}\frac{\partial \widehat{\mathbf{K}}_{je}}{\partial \rho_e}\mathbf{T}_{je}\mathbf{u}_{je} = -\mathbf{u}_{je}^{\mathrm{T}}\frac{\partial \mathbf{k}_{je}}{\partial \rho_e}\mathbf{u}_{je} \tag{43}$$

where $\mathbf{T}_{je}$ is the interpolation wavelet transformation relating single and multiscaled element nodal vectors $\hat{\mathbf{u}}_{je}$ and $\mathbf{u}_{je}$ at resolution j. (Note that the array size of $\hat{\mathbf{u}}_{je}$ is not the same as that of $\mathbf{u}_{je}$ in general.)

Now, using Eqs. (40a), (42) and (43), both the design optimization and the analysis can be processed in the multiscale multiresolution setting. The actual implementation algorithm is described in Fig. 16. In the present multiscale multiresolution setting, the results obtained in the previous resolution level for both analysis and design optimization are used as the initial guess at the next higher resolution level.

3.4. Numerical examples

Here, we will consider two benchmark-type compliance minimization problems set up in the context of topology optimization. As an optimizer, we use the feasible direction method provided in DOT (Vanderplaats, 1995). Since the role and effectiveness of the multiscale topology optimization are discussed in earlier papers such as Kim and Yoon (2000, 2001), Poulsen (2002), Earmme (2001), Yoon et al. (2003), we will be mainly concerned with the numerical aspect of the multiscale wavelet-Galerkin application to multiscale topology optimization.

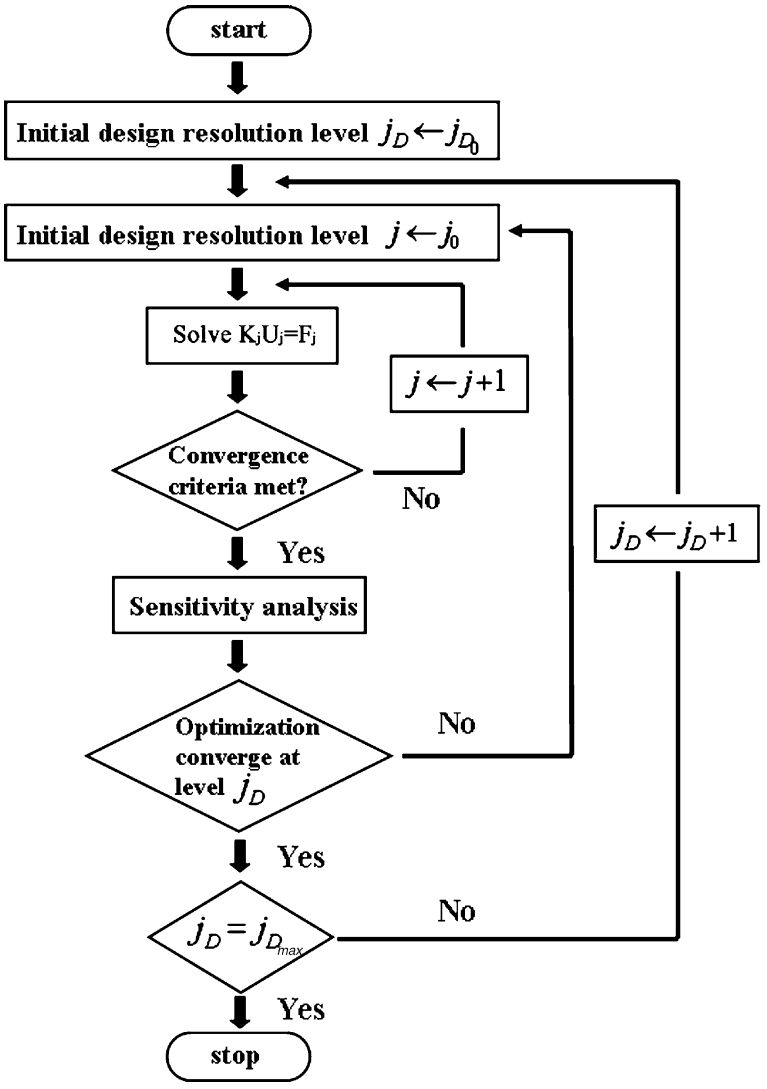

Fig. 16. The algorithm for the present multiscale analysis and design optimization.

Design Example 1. First, we consider the topology optimization depicted in Fig. 17. Unless stated otherwise, we will use the following values for all examples: Young's modulus, $E = 2 \times 10^7$, Poisson's ratio, $v = 0.3$. The constraint ratio is 37.5%. The results shown in Fig. 18 are almost the same as those shown in Kim and Yoon (2000). However, Kim and Yoon (2000) used the single-scale finite element analysis with the full analysis resolution consistent with the final design resolution $j_D = 5$. To emphasize the role of the present adaptive wavelet-Galerkin method, we show in Fig. 19(a) how the number of analysis degrees of freedom varies at the design resolution level $j_D = 3$. Fig. 19(b)–(d) shows the locations of the interpolation points at the final analysis step for N_{iter} (iteration number) = 1, 3, and 6. As in the previous analysis results of Figs. 10 and 13, the horizontal and vertical displacements shown in Fig. 19 are interpolated at different locations, which also contribute to the reduction of the total number of the necessary degrees of freedom.

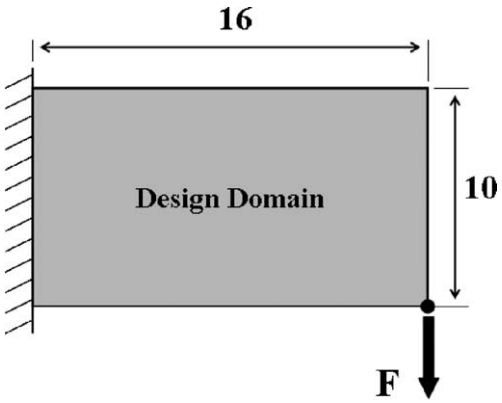

Fig. 17. Compliance minimization of a short cantilever beam subject to a point force at the right end corner.

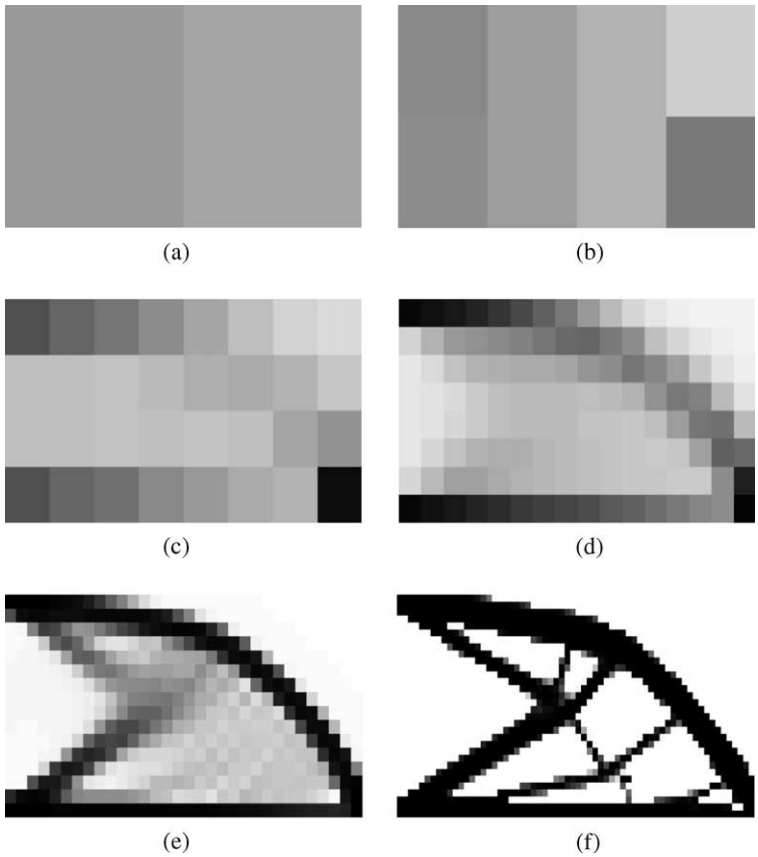

Fig. 18. The optimized results at the various design resolution levels j_D. The final optimized design is shown in (f). (a) $j_D = 0$, $N_{\text{iter}} = 4$; (b) $j_D = 1$, $N_{\text{iter}} = 5$; (c) $j_D = 2$, $N_{\text{iter}} = 6$; (d) $j_D = 3$, $N_{\text{iter}} = 6$; (e) $j_D = 4$, $N_{\text{iter}} = 9$; (f) $j_D = 5$, $N_{\text{iter}} = 40$ (N_{iter} = the total number of the design iteration, circle: points where gradients are evaluated).

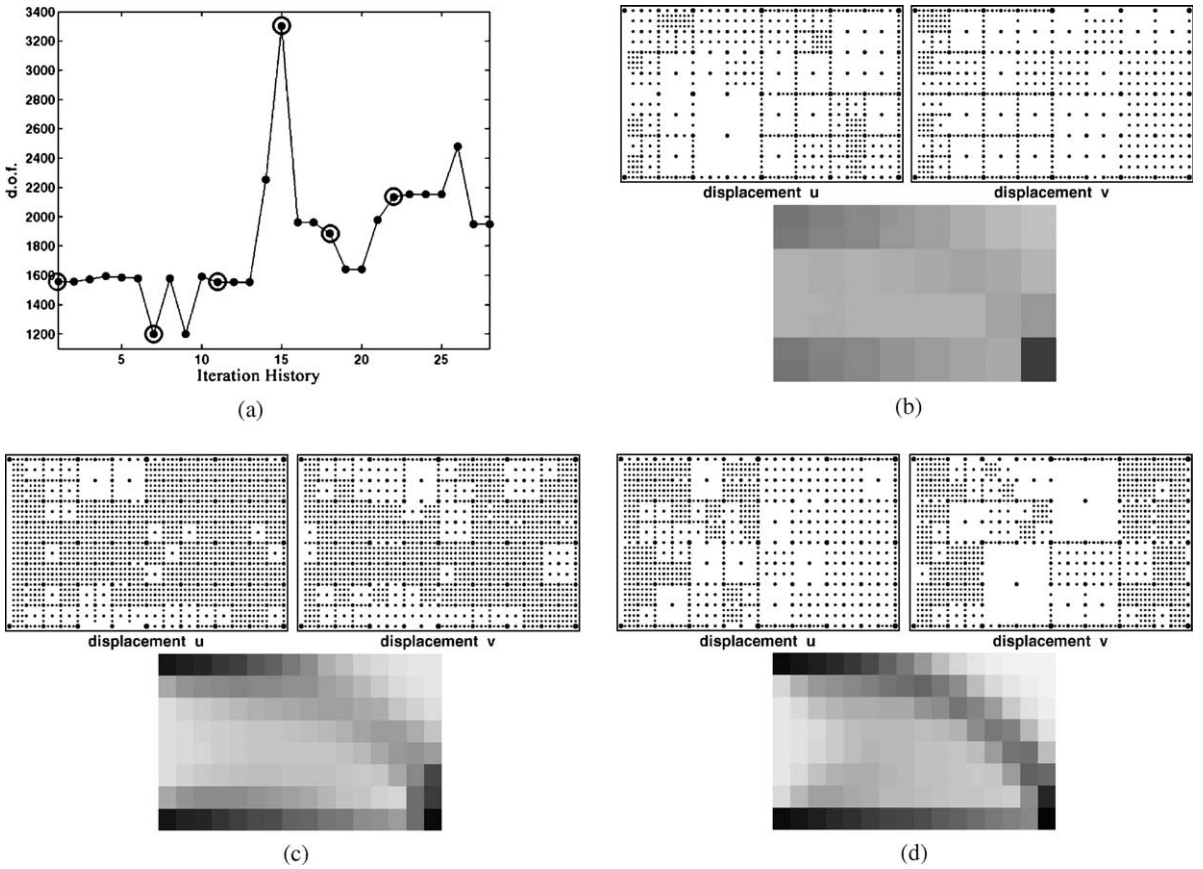

Fig. 19. The analysis history for the design resolution level $j_D = 3$: (a) the history of the number of analysis degrees of freedom (circle is marked every one iteration); (b)–(d) the interpolation points after the first, third and sixth iterations.

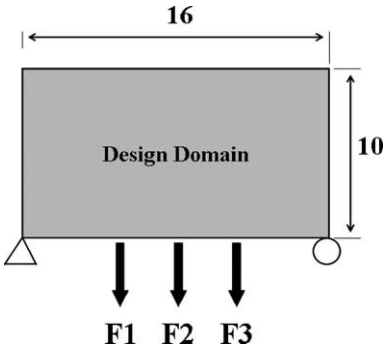

Fig. 20. Compliance minimization of a structure subject to three simultaneously acting loads.

Design Example 2. As the next design example, a compliance minimization problem depicted in Fig. 20 is considered for simultaneously acting loads $F_1 = F_2 = F_3$. The volume ratio is 30%.

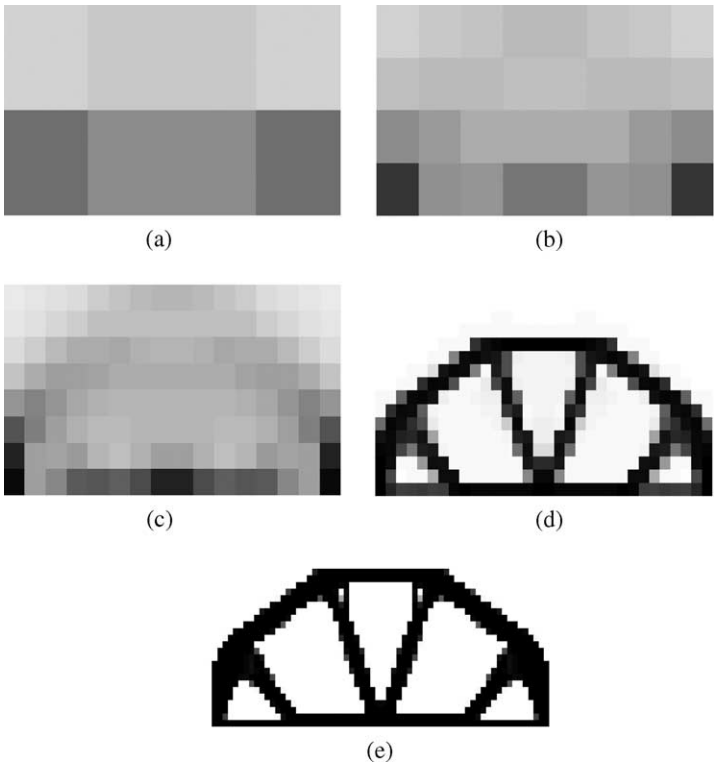

Fig. 21. The optimized results at various design resolution levels for the design problem depicted in Fig. 20: (a) $j_D = 1$, (b) $j_D = 2$, (c) $j_D = 3$, (d) $j_D = 4$, and (e) $j_D = 5$ (final).

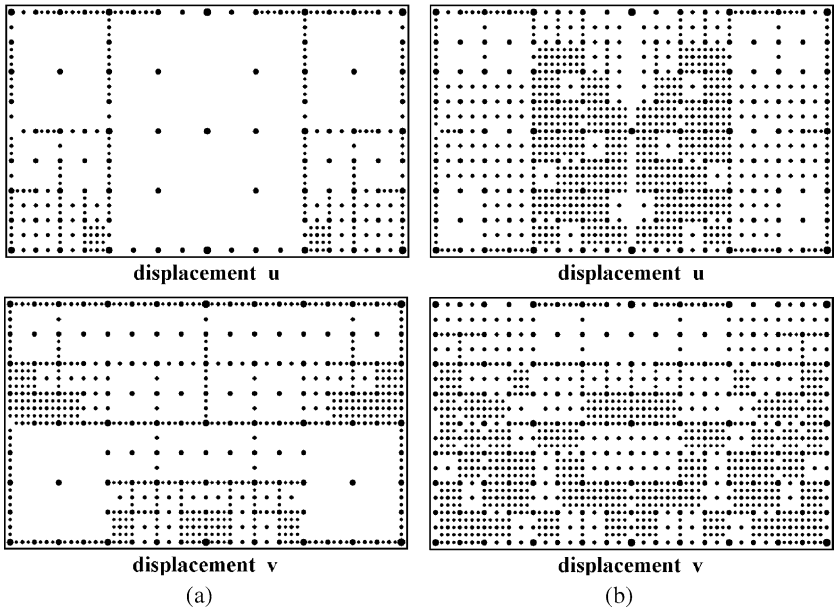

Fig. 22. The location of adaptively inserted interpolation points after completing the design levels of (a) $j_D = 2$ and (b) $j_D = 4$.

The optimized designs are shown in Fig. 21 and typical locations of interpolation points are illustrated in Fig. 22. Fig. 22 shows how effective the present adaptive strategy is. We have also studied other topology optimization problems using the present approach and obtained satisfactory results similar to those obtained for Design Examples 1 and 2.

4. Conclusions

The multiscale wavelet-Galerkin method for two-dimensional elasticity problems has been developed. The intrinsic multiscale characteristics of wavelets allowed an easy implementation of an adaptive strategy which successfully reduced the total number of analysis degrees of freedom. As an adaptive solver, the wavelet-Galerkin method was successfully applied to the multiscale topology design optimization. The adaptive analysis reduced the analysis matrix size but did not affect the quality of optimized designs. If design optimization and analysis are fully integrated in the frame of the multiscale multiresolution setting, not only the analysis resolution but also design optimization resolution can be adaptively adjusted. The full development of the multiscale method for design problem is expected to allow design optimization that does not require the pre-selected resolution levels of analysis and design optimization.

References

Amaratunga, K., Williams, J.R., 1997. Wavelet-Galerkin solutions of boundary value problems. Arch. Comput. Methods Engng. 4, 243–285.

Bendsøe, M.P., Kikuchi, N., 1988. Generating optimal topologies in structural design using a homogenization method. Comput. Methods Appl. Mech. Engng. 71, 197–224.

Bendsøe, M.P., Sigmund, O., 1999. Material interpolation schemes in topology optimization. Arch. Appl. Mech. 69, 635–654.

Bendsøe, M.P., 1995. Optimization of Structural Topology, Shape and Material. Springer, Berlin, Heidelberg.

Bertoluzza, S., Naldi, G., 1996. A wavelet collocation method for the numerical solution of partial differential equations. Appl. Comput. Harmonic Anal. 3, 1–9.

Bertoluzza, S., 1997. An adaptive collocation method based on interpolating wavelets. In: Dahmen, W., Kurdila, A.J., Oswald, P. (Eds.), Multiscale Wavelet Methods for PDEs. Academic Press, San Diego, pp. 109–135.

Beylkin, G., Saito, N., 1993. Multiresolution representations using the autocorrelation functions of compactly supported wavelets. IEEE Trans. Signal Process. 41, 3584–3590.

Christon, M.A., Roach, D.W., 2000. The numerical performance of wavelets for PDEs: the multi-scale finite element. Comput. Mech. 25, 230–244.

Cohen, A., Dahmen, W., DeVore, R., 1998. Adaptive wavelet methods for elliptic operator equations—convergence rates. RWTH Aachen, IGPM Preprint No. 165.

Cohen, A., Masson, R., 1999. Wavelet methods for second order elliptic problems-preconditioning and adaptivity. SIAM J. Sci. Comput. 21, 1006–1026.

Dahmen, W., 2001. Wavelet methods for PDEs—some recent developments. J. Comput. Appl. Math. 128, 133–185.

DeRose Jr., G., 1998. Solving topology optimization problems using wavelet-Galerkin techniques. Ph.D. Thesis, Michigan State University.

Diaz, A.R., 1999. A wavelet-Galerkin scheme for analysis of large-scale problems on simple domains. Int. J. Numer. Methods Engng. 44, 1599–1616.

Earmme, T.M., 2001. The role of the wavelet basis in multiscale topology optimization. M.S. Thesis, School of Mechanical and Aerospace Engineering, Seoul National University, Korea.

Eshenauer, H.A., Olhoff, N., 2001. Topology optimization of continuous structures: a review. Appl. Mech. Rev. 54 (4), 331–389.

Glowinski, R., Rieder, A., Wells Jr., R.O., Zhou, X., 1993. A Wavelet multi-grid preconditioner for Dirichlet boundary value problems in general domains. Technical Report, Computational Mathematics Lab, TR93-06, Rice University.

Glowinski, R., Pan, T.W., Wells Jr., R.O., Zhou, X., 1994. Wavelet and finite element solutions for the Neumann problem using fictitious domains. Technical Report, Computational Mathematics Lab, Rice University.

Jang, G.W., Kim, J.E., Kim, Y.Y., 2003. Multiscale Galerkin method using interpolation wavelets for two-dimensional elliptic problems in general domains. Int. J. Numer. Methods Engng., in press.

Kim, Y.Y., Jang, G.W., 2002. Interpolation wavelet-based multi-scale Galerkin method for thin-walled box beam analysis. Int. J. Numer. Methods Engng. 53, 1575–1592.

Kim, Y.Y., Yoon, G.H., 2000. Multi-resolution multi-scale topology optimization—a new paradigm. Int. J. Solids Struct. 37, 5529–5559.

Kim, Y.Y., Yoon, G.H., 2001. Multiscale multiresolution topology optimization in general domains using a subdivision method. In: CD-ROM Proceeding of the Fourth World Congress of Structural and Multidisciplinary Optimization, June 4–8, 2001, Dalian, China, pp. 40–41.

Mallat, S., 1998. A Wavelet Tour of Signal Processing. Academic Press, New York.

Monasse, P., Perrier, V., 1998. Orthonormal wavelet bases adapted for partial differential equations with boundary conditions. SIAM J. Math. Anal. 29 (4), 1040–1065.

Poulsen, T.A., 2002. Topology optimization in wavelet space. Int. J. Numer. Methods Engng. 53, 567–582.

Stollnitz, E.J., DeRose, T.D., Salesin, D.H., 1996. Wavelets for Computer Graphics: Theory and Applications. Morgan Kaufmann Publishers, San Francisco. pp. 21–31.

Vanderplaats, G.N., 1995. DOT—Design Optimization Tools User's Manual, Vanderplaats Research & Development, Inc.

Wells Jr., R.O., Zhou, X., 1993. Wavelet solutions for the Dirichlet problem. Technical Report, Computational Mathematics Lab, Rice University.

Yoon, G.H., Kim, Y.Y., Bendsøe, M.P., Sigmund, O., 2003. Hinge-free topology optimization with an embedded translation-invariant wavelet shrinkage method, Struct. Optim., in press.

Zienkiewicz, O.C., Zhu, J.Z., 1992. The superconvergent patch recovery and a posteriori error estimates. Part 1: the recovery technique. Int. J. Numer. Mech. Engng. 33, 1331–1364.